Sensors and Materials, Vol. 36, No. 7 (2024) 2727–2733
MYU Tokyo

Letter

S & M 3697

Slope-assisted Configuration for Fiber-optic Multimodal Interference Temperature Sensing

Motoki Sano,[1] Kohei Noda,[2] Heeyoung Lee,[3] and Yosuke Mizuno[1,4*]

[1]Faculty of Engineering, Yokohama National University, Yokohama 240-8501, Japan
[2]Graduate School of Engineering, The University of Tokyo, Tokyo 113-8656, Japan
[3]Graduate School of Engineering and Science, Shibaura Institute of Technology, Tokyo 135-8548, Japan
[4]Institute of Multidisciplinary Sciences, Yokohama National University, Yokohama 240-8501, Japan

(Received May 7, 2024; accepted June 5, 2024)

Keywords: optical fiber sensors, multimode interference, temperature sensing

We present a slope-assisted configuration for fiber-optic temperature sensing using multimodal interference (MMI) in a single-mode–multimode–single-mode structure. By measuring the power in the slope of the MMI spectrum, this method overcomes conventional limitations, enabling high-speed temperature measurement without the need for wavelength sweeping. The operational principles of this technique are described in detail, and a thorough evaluation of its limitations is conducted.

1. Introduction

Fiber-optic temperature sensors are distinguished by their unique characteristics, including compactness, lightweight construction, rapid response times, remote sensing capabilities, and immunity to interference from ambient electromagnetic fields.[1–4] A variety of these sensors have been developed, each utilizing different principles such as fiber Bragg gratings,[5–7] long-period gratings,[8,9] Brillouin scattering,[10–12] Raman scattering,[12] surface plasmon resonance,[13] and others.[14] While each technique offers its own set of advantages, some may also present challenges, including the requirement for specialized equipment, high costs, complex fabrication, or reduced stability. Among the available approaches, one that stands out for its simplicity and cost-effectiveness is based on the multimodal interference (MMI) effect, known as the single-mode–multimode–single-mode (SMS) fiber sensor.[15–26] This SMS-based configuration, implemented using a multimode fiber (MMF) sandwiched between two single-mode fibers (SMFs), has been widely explored and reported in various sensing scenarios. The appeal of this method lies in its accessibility and adaptability, making it a valuable addition to the diverse landscape of fiber-optic temperature sensing technologies.

Liu and Wei,[16] using the SMS structure, achieved a strain sensitivity of −18.6 pm/με and a temperature sensitivity of +58.5 pm/°C using a 1.8-m-long graded-index (GI) silica MMF at 1550 nm band. Tripathi *et al.*[17] demonstrated that the absolute values and signs of strain and

*Corresponding author: e-mail: mizuno-yosuke-rg@ynu.ac.jp
https://doi.org/10.18494/SAM5134

ISSN 0914-4935
https://myukk.org/

temperature sensitivities considerably depend on the MMF's structure and material. Furthermore, Huang *et al.*[18] introduced a 0.16-m-long polymer optical fiber (POF) based on polymethyl methacrylate (PMMA) as the MMF, suitable for measuring larger strains, and obtained a strain sensitivity of −2.82 pm/με and a temperature sensitivity of +93.1 pm/°C at 1570 nm band. In our previous work,[19,20] we achieved extraordinarily high sensitivities of −112 pm/με for strain and +49.8 nm/°C for temperature using a 1.0-m-long, 62.5-μm-core-diameter perfluorinated GI-POF at 1300 nm band. A no-core fiber was also used as the MMF in the SMS structure.[25,26] These modal-interference-based sensors conventionally estimated strain or temperature from the dips or peaks of the transmission spectrum of broadband light, measured by an optical spectrum analyzer (OSA). However, the relatively slow wavelength sweeping of the OSA made the real-time acquisition of strain or temperature information challenging.

In this study, we focus on temperature measurement and propose a method utilizing the slope of the multimodal interference spectrum. This approach, which does not require the wavelength sweeping of an OSA, enables high-speed operation.

In SMS-based MMI sensing, when light is injected, it is channeled through the input SMF into the MMF section. Here, the first few modes within the MMF are excited, triggered by the disparity in spot size between the fundamental modes of the SMF and MMF. Upon reaching the second conjunction of the MMF/SMF, these modes are coupled back into the fundamental mode of the output SMF. The power in the output SMF (P_{out}) can be expressed as[17]

$$P_{out} \propto \left| a_0^2 + a_1^2 e^{i(\beta_0-\beta_1)L} + a_2^2 e^{i(\beta_0-\beta_2)L} + \cdots \right|^2 . \tag{1}$$

Here, a_i represents the field amplitude of the i-th mode at the initial SMF/MMF boundary, β_i is the propagation constant of the i-th mode, and L is the length of the MMF. It is evident from this expression that P_{out} is affected by the temperature applied to the MMF, which affects both β_i (thermo-optic coefficients vary among different propagation modes) and L. Consequently, temperature sensing can be achieved by monitoring shifts in the spectral locations of peaks (or dips).

Conventionally, strain and temperature sensing using SMS-based MMI has been generally realized by directly measuring the shift in the interference spectral pattern of transmitted broadband light.[15–20] Note that some exceptions using edge filters[21,22] and machine learning[23,24] have been reported, but their signal processing methods are relatively complex. In standard configurations, owing to the necessity of wavelength sweeping of an OSA, high-speed measurement was challenging. In contrast, the slope-assisted measurement method proposed in this study utilizes the zero-span function of the OSA, observing the temporal variation of spectral power at a fixed wavelength, which is much simpler than the edge-filter-based methods.[21,22] This eliminates the need for wavelength sweeping, enabling high-speed measurement. Note that the slope-assisted high-speed configurations have been used in numerous other sensing techniques.[27–33]

2. Materials and Mehtod

The experimental setup used to verify this method is shown in Fig. 1. The broadband light emitted from a supercontinuum light source (SC-5, Yangtze Soton Laser; refer to Fig. 2 of Ref. 34 for its wideband output spectrum) was injected into an SMS structure containing a 0.5-m-long silica MMF, and the transmitted light was observed with an OSA (AQ6370D, Yokogawa Electric). A 0.1-m-long section of the MMF was heated with a hot plate to observe temperature dependence. By multiplying the obtained temperature coefficient by a factor of 5 (equivalent to 0.5/0.1), the temperature coefficient for heating the entire length can be calculated. Note that in the context of SMS-based MMI, the sensor's response is predicated on the basis of the average temperature along the entire length of the MMF. This implies that the effect of temperature on the transmitted spectrum remains consistent whether a uniform temperature alteration is applied across the full length of the MMF or if a temperature change of magnitude k is applied to a $1/k$ fraction of the MMF's total length.[34]

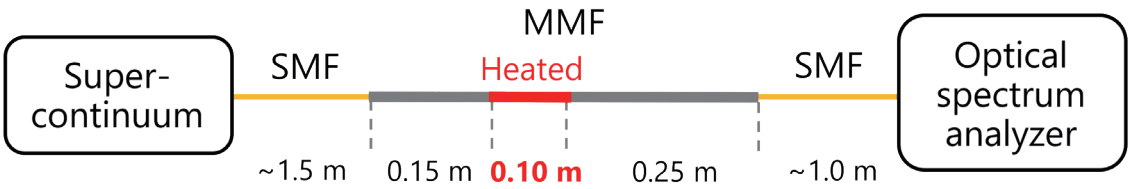

Fig. 1. (Color online) Experimental setup of SMS-based MMI temperature sensor for characterizing the slope-assisted configuration.

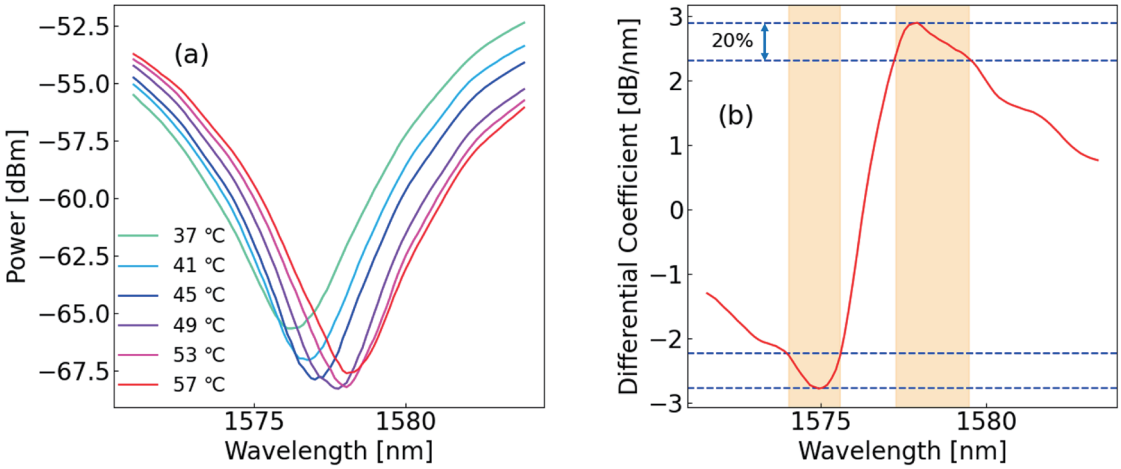

Fig. 2. (Color online) (a) Temperature dependence of the transmitted spectrum. (b) Differential coefficient of the spectrum (measured at 37 v°C) at each wavelength. The linear regions are indicated.

3. Results

The temperature dependence of the transmitted spectrum near the dip around 1575 nm is shown in Fig. 2(a). With increasing temperature, the dip shifted to the longer wavelength side and the power tended to decrease (which is reasonable considering the nature of MMI). The temperature dependence of the dip wavelength was almost linear, with a dependence coefficient of +98.0 pm/°C. It was also confirmed that the spectral shape returned to its original state when the temperature was lowered. Note that the spectral power is comparatively subdued, primarily owing to the lower output power of the light source around this particular wavelength. Utilizing an amplified spontaneous emission source, for instance, would serve to increase the spectral power.

Subsequently, to evaluate the slope of the transmitted spectrum at 37 °C, the results of differentiation with respect to wavelength are shown in Fig. 2(b). At no points is the slope constant with respect to wavelength, thereby precluding the presence of perfectly linear regions. Here, "linear" regions are designated as those intervals where the absolute values decrease by 20% around the minimum and maximum values. The linear region on the short-wavelength side of the dip was 1574.28–1575.71 nm, and on the long-wavelength side, it was 1577.27–1579.48 nm.

Finally, the temperature dependences of the powers at the longest wavelengths in the two linear regions are shown in Figs. 3(a) (1575.71 nm) and 3(b) (1579.48 nm). These specific wavelengths were chosen owing to their extensive temperature dynamic ranges, under the assumption that temperature variations ascend exclusively from the baseline temperatures. Both dependences were roughly linear with coefficients of 0.22 and −0.38 dB/°C, respectively. The deviations from the linear trends can be attributed to the changes in dip power. On the other hand, the temperature dependences of the powers at the central wavelengths of the linear ranges are shown in Figs. 4(a) (1575.45 nm) and 4(b) (1578.31 nm). The temperature dependence

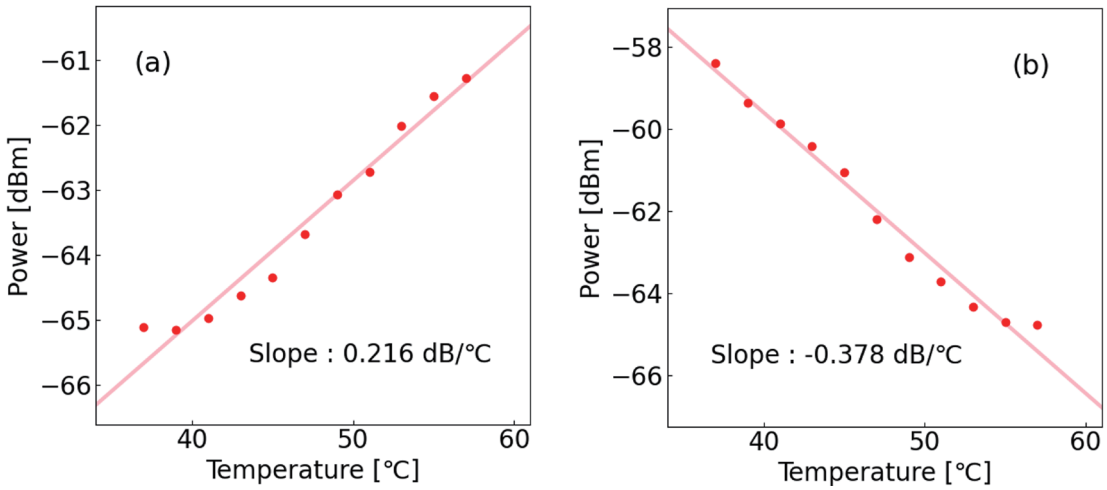

Fig. 3. (Color online) Temperature dependences of the spectral power at (a) 1575.71 and (b) 1579.48 nm. The solid lines are linear fits.

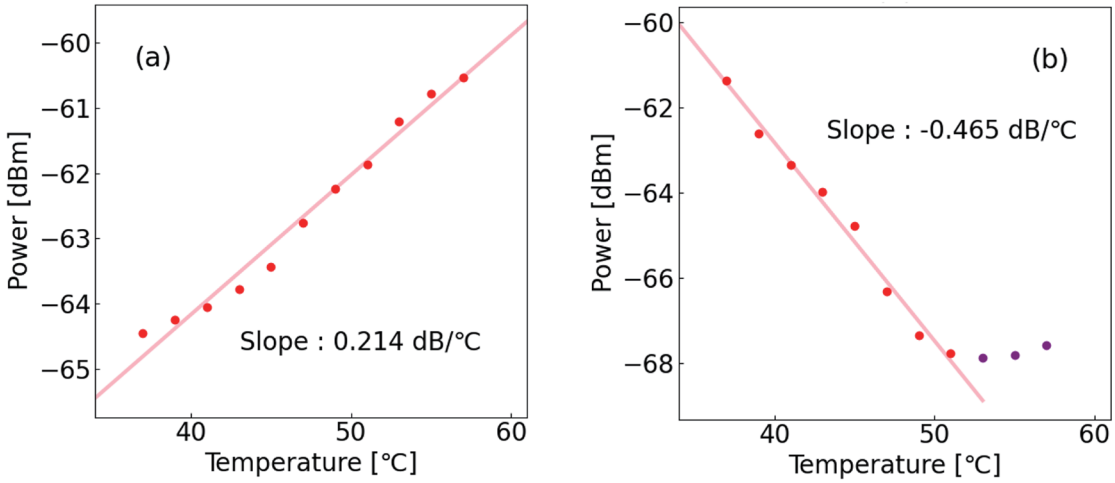

Fig. 4. (Color online) Temperature dependences of the spectral power at (a) 1575.45 and (b) 1578.31 nm. The solid lines are linear fits (of the red points).

coefficients are 0.21 and −0.47 dB/°C, respectively, but in the long-wavelength side [Fig. 4(b)], the dependence was not linear at higher temperatures, limiting the temperature dynamic range. A comparison with previous publications regarding temperature sensitivities is generally important, but a fair quantitative comparison is challenging in this configuration because sensitivities vary with wavelength, fiber length, and other factors. Note that normalizing the sensitivities is difficult owing to the presence of critical wavelengths[17] and the non-monotonic dependence on fiber length.[35] Thus, it was shown that, by selecting an appropriate wavelength and measuring the power in the slope of the MMI spectrum, we can translate the observed values into changes in temperature (within a certain temperature dynamic range). This method is inherently capable of real-time operation.

4. Discussion and Conclusion

In this study, we developed and validated a slope-assisted configuration for fiber-optic SMS-based temperature sensing, exploiting the characteristics of the MMI spectrum. By circumventing the constraints inherent to conventional wavelength sweeping techniques, the proposed method facilitates real-time temperature measurement. Experimental findings confirm the method's capability to translate observed spectral powers into temperature changes. It is important to acknowledge a limitation of this approach, namely, its susceptibility to inaccuracies in temperature measurement when optical loss occurs within the fibers or when fluctuations in the output power of the light source are present (reflecting a trade-off relationship between measurement speed and accuracy). A potential solution to this challenge may lie in the implementation of a dual-slope-assisted configuration,[31–33] although this may further constrain the temperature dynamic range. In addition, the long-term stability poses a challenge; significant strain or temperature changes can substantially alter the transmitted spectrum, necessitating a

reevaluation to identify an appropriate wavelength for use. While theoretically feasible, automating this process could prove complex. Notwithstanding these challenges, we believe that our method will be an important step toward the development of practical high-speed sensors exploiting SMS-based MMI in the future.

Acknowledgments

This work was partially supported by the Japan Society for the Promotion of Science (JSPS) KAKENHI (Grant Nos. 21H04555, 22K14272, and 20J22160).

References

1 K. T. V. Grattan and B. T. Meggitt: Optical Fiber Sensor Technology: Fundamentals (Springer, New York, 2000).
2 A. H. Hartog: An Introduction to Distributed Optical Fibre Sensors (CRC Press, Boca Raton, 2017).
3 G. P. Agrawal, Nonlinear Fiber Optics (Academic Press, New York, 1995).
4 M. Niklès and F. Ravet: Nat. Photonics **4** (2010) 431. https://doi.org/10.1038/nphoton.2010.149
5 K. O. Hill and G. Meltz: J. Lightwave Technol. **15** (1997) 1263. https://doi.org/10.1109/50.618320
6 R. Ishikawa, H. Lee, A. Lacraz, A. Theodosiou, K. Kalli, Y. Mizuno, and K. Nakamura: Jpn. J. Appl. Phys. **57** (2018) 038002. http://doi.org/10.7567/JJAP.57.038002
7 D. Paladino, G. Quero, C. Caucheteur, P. Mégret, and A. Cusano: Opt. Express **18** (2010) 10473. https://doi.org/10.1364/OE.18.010473
8 Y. Wang: J. Appl. Phys. **108** (2010) 081101. https://doi.org/10.1063/1.3493111
9 C.-L. Zhao, L. Xiao, J. Ju, M. S. Demokan, and W. Jin: J. Lightwave Technol. **26** (2007) 220. https://doi.org/10.1109/JLT.2007.911106
10 Y. Mizuno, N. Hayashi, H. Fukuda, K. Y. Song, and K. Nakamura: Light Sci. Appl. **5** (2016) e16184. http://dx.doi.org/10.1038/lsa.2016.184
11 M. A. Soto, J. A. Ramírez, and L. Thévenaz: Nat. Commun. **7** (2016) 10870. https://doi.org/10.1038/ncomms10870
12 M. N. Alahbabi, Y. T. Cho, and T. P. Newson: Opt. Lett. **30** (2005) 1276. https://doi.org/10.1364/OL.30.001276
13 T. Cheng, B. Li, F. Zhang, J. Chen, Q. Zhang, X. Yan, X. Zhang, T. Suzuki, Y. Ohishi, and F. Wang: IEEE Sens. J. **22** (2022) 3246. https://doi.org/10.1109/JSEN.2022.3141239
14 A. Micco, A. Ricciardi, G. Quero, A. Crescitelli, W. J. Bock, and A. Cusano: Opt. Lett. **39** (2014) 861. https://doi.org/10.1364/OL.39.000861
15 A. Mehta, W. Mohammed, and E. G. Johnson: IEEE Photonics Technol. Lett. **15** (2003) 1129. https://doi.org/10.1109/LPT.2003.815338
16 Y. Liu and L. Wei: Appl. Opt. **46** (2007) 2516. https://doi.org/10.1364/AO.46.002516
17 S. M. Tripathi, A. Kumar, R. K. Varshney, Y. B. P. Kumar, E. Marin, and J. P. Meunier: J. Lightwave Technol. **27** (2009) 2348. https://doi.org/10.1109/JLT.2008.2008820
18 J. Huang, X. Lan, H. Wang, L. Yuan, T. Wei, Z. Gao, and H. Xiao: Opt. Lett. **37** (2012) 4308. https://doi.org/10.1364/OL.37.004308
19 G. Numata, N. Hayashi, M. Tabaru, Y. Mizuno, and K. Nakamura: IEEE Photonics J. **6** (2014) 6802306. http://dx.doi.org/10.1109/JPHOT.2014.2352637
20 G. Numata, N. Hayashi, M. Tabaru, Y. Mizuno, and K. Nakamura: Appl. Phys. Express **8** (2015) 072502. http://dx.doi.org/10.7567/APEX.8.072502
21 A. M. Hatta, Y. Semenova, G. Rajan, P. Wang, J. Zheng, and G. Farrell: Opt. Commun. **283** (2010) 1291. https://doi.org/10.1016/j.optcom.2009.11.020
22 A. M. Hatta, Y. Semenova, and G. Farrell: Microwave Opt. Technol. Lett. **55** (2013) 1645. https://doi.org/10.1002/mop.27619
23 Y.-N. Pang, B. Liu, J. Liu, S-P. Wan. A. Wu, J. Yuan, X. Xin, X.-D. He, and Q. Wu: J. Lightwave Technol. **40** (2022) 4443. https://doi.org/10.1109/JLT.2022.3155194
24 K. Toda, K. Kishizawa, Y. Toyoda, K. Noda, H. Lee, K. Nakamura, K. Ichige, and Y. Mizuno: Appl. Phys. Express **15** (2022) 072002. https://doi.org/10.35848/1882-0786/ac749e

25 Q. Meng, X. Dong, K. Ni, Y. Li, B. Xu, and Z. Chen: IEEE Sens. J. **14** (2014) 1813. https://doi.org/10.1109/JSEN.2014.2298511
26 Y. Zhao, J. Zhao, and Q. Zhao: Sens. Actuators, A. **313** (2020) 112160. https://doi.org/10.1016/j.sna.2020.112160
27 Y. Peled, A. Motil, L. Yaron, and M. Tur: Opt. Express **19** (2011) 19845. https://doi.org/10.1364/OE.19.019845
28 H. Lee, N. Hayashi, Y. Mizuno, and K. Nakamura: IEEE Photonics J. **8** (2016) 6802807. http://dx.doi.org/10.1109/JPHOT.2016.2562512
29 H. Lee, K. Nakamura, and Y. Mizuno: Opt. Fiber Technol. **59** (2020) 102312. https://doi.org/10.1016/j.yofte.2020.102312
30 J. Li, X. Zhou, Y. Xu, L. Qiao, J. Zhang, and M. Zhang: Photonics Res. **10** (2022) 205. https://doi.org/10.1364/PRJ.442352
31 D. Ba, B. Wang, D. Zhou, M. Yin, Y. Dong, H. Li, Z. Lu, and Z. Fan: Opt. Express **24** (2016) 9781. https://doi.org/10.1364/OE.24.009781
32 B. Wang, X. Fan, Y. Fu, and Z. He: J. Lightwave Technol. **37** (2019) 4573. https://doi.org/10.1109/JLT.2019.2912746
33 Y. Suzuki, H. Lee, H. Sasage, K. Noda, K. Nakamura, and Y. Mizuno: Jpn. J. Appl. Phys. **62** (2023) 108005. https://doi.org/10.35848/1347-4065/acfa4c
34 Y. Mizuno, S. Hagiwara, T. Kawa, H. Lee, and K. Nakamura: Jpn. J. Appl. Phys. **57** (2018) 058002. https://doi.org/10.7567/JJAP.57.058002
35 T. Kawa, G. Numata, H. Lee, N. Hayashi, Y. Mizuno, and K. Nakamura: IEICE Electron. Express **14** (2017) 20161239. http://doi.org/10.1587/elex.14.20161239